SUPPLEMENTARY INFORMATION

Spatial arrangement of functional domains in OxyS stress response sRNA

Vesna Štih[1,2], Heinz Amenitsch[3], Janez Plavec[1,2,4,*] and Peter Podbevšek[1,*]

[1] Slovenian NMR Centre, National Institute of Chemistry, Hajdrihova 19, SI-1000 Ljubljana, Slovenia

[2] Faculty of Chemistry and Chemical Technology, University of Ljubljana, Večna pot 113, SI-1000 Ljubljana, Slovenia

[3] Institute of Inorganic Chemistry, Graz University of Technology, Stremayrgasse 9, 8010 Graz, Austria

[4] EN-FIST Centre of Excellence, Trg OF 13, SI-1000 Ljubljana, Slovenia

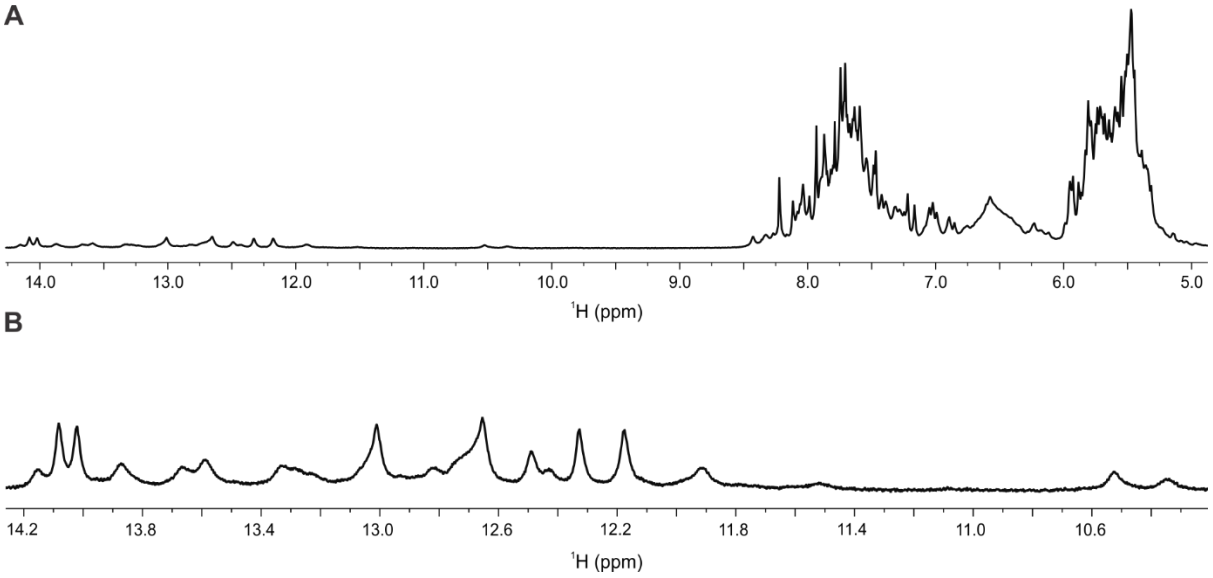

Figure S1. ^{1}H NMR spectrum of OxyS. **(A)** Imino, aromatic and anomeric region. **(B)** Close-up of the imino region (10.2 – 14.3 ppm). The spectrum was acquired at 25 °C with 90 % H_2O and 10 % ^2H_2O, 1 mM RNA concentration, 15 mM Na-phosphate buffer, 30 mM NaCl, and, pH 6, on a 600 MHz NMR spectrometer.

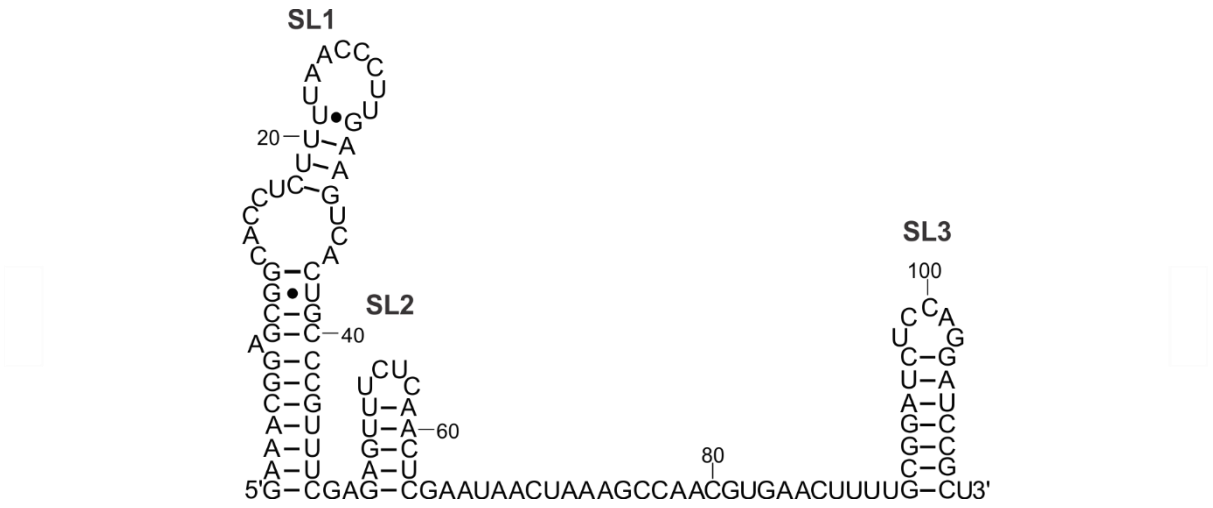

Figure S2. Secondary structure of OxyS RNA as predicted by Mfold (Zuker 2003). The structure shown has the lowest energy (dG=-33.50 kcal/mol).

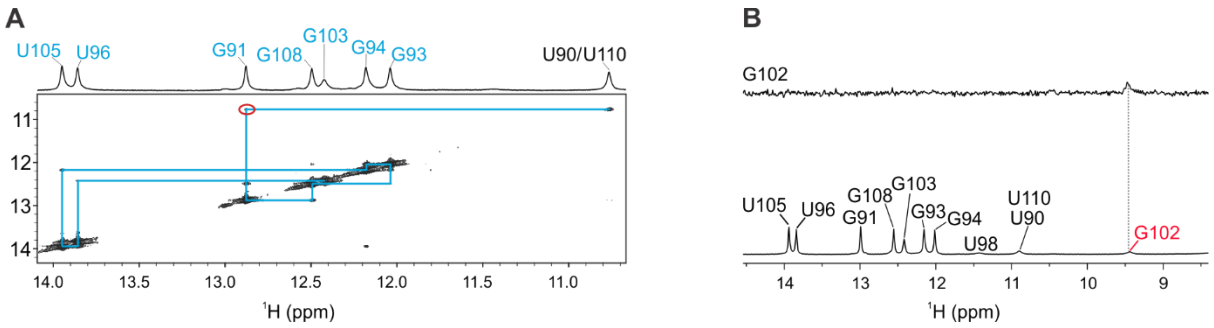

Figure S3. Evaluating U90·U110 and G102·U98 mismatch formation. **(A)** NOESY spectrum (τ_m = 200 ms) of $SL3_{ext}$. Cross-peak between U90/U110 and G91 is denoted with a red circle. **(B)** ^{1}H NMR spectrum and 1D ^{15}N-edited HSQC spectra of site-specific isotopically enriched SL3. Spectra were acquired at 5 °C with 90 % H_2O and 10 % $^{2}H_2O$, 1 mM RNA concentration, 15 mM Na-phosphate buffer, 30 mM NaCl, and, pH 6, on a 600 MHz NMR spectrometer.

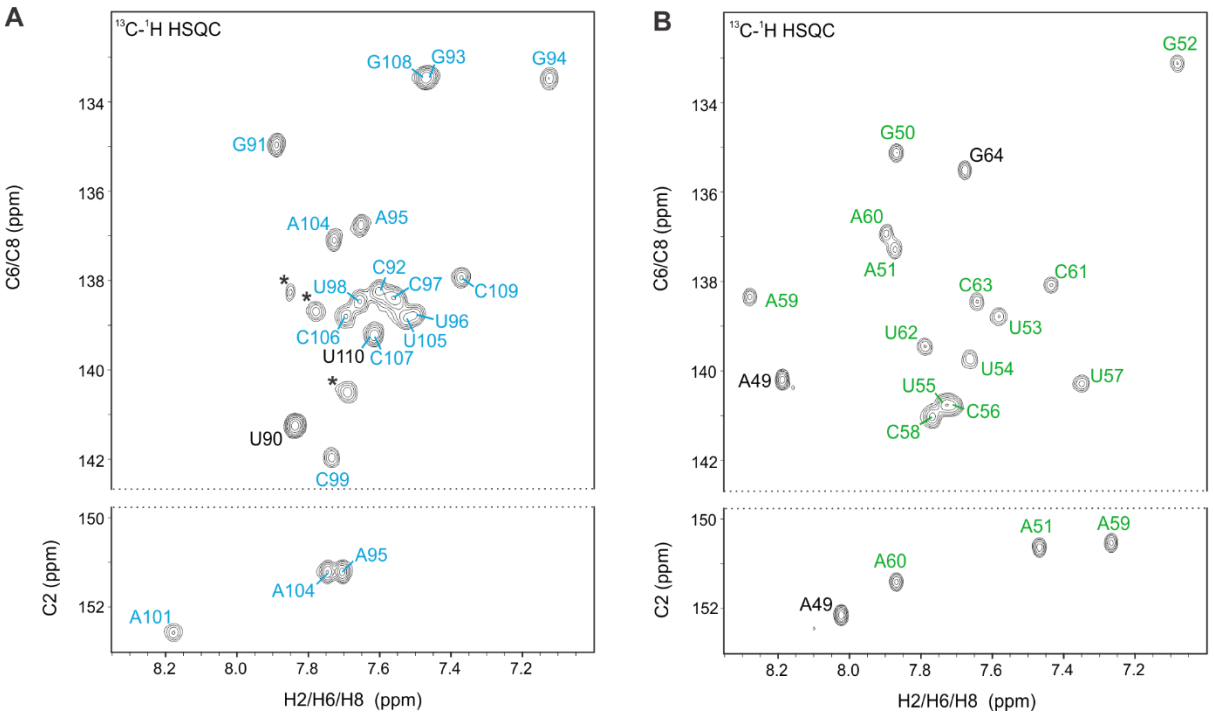

Figure S4. (A) 2D ^{13}C-^{1}H HSQC spectra of SL3. Unassigned peaks are denoted with asterisk and correspond to either C100, A101, G102 or G103. **(B)** 2D ^{13}C-^{1}H HSQC spectra of SL2 with assignments of all nucleotides. Nucleotides which were added at 5' and 3' end to protect the closing base pair are in coloured in black. Spectra were acquired at 25 °C with 90 % H_2O and 10 % $^{2}H_2O$, 1 mM RNA concentration, 15 mM Na-phosphate buffer, 30 mM NaCl, and, pH 6, on a 600 MHz NMR spectrometer.

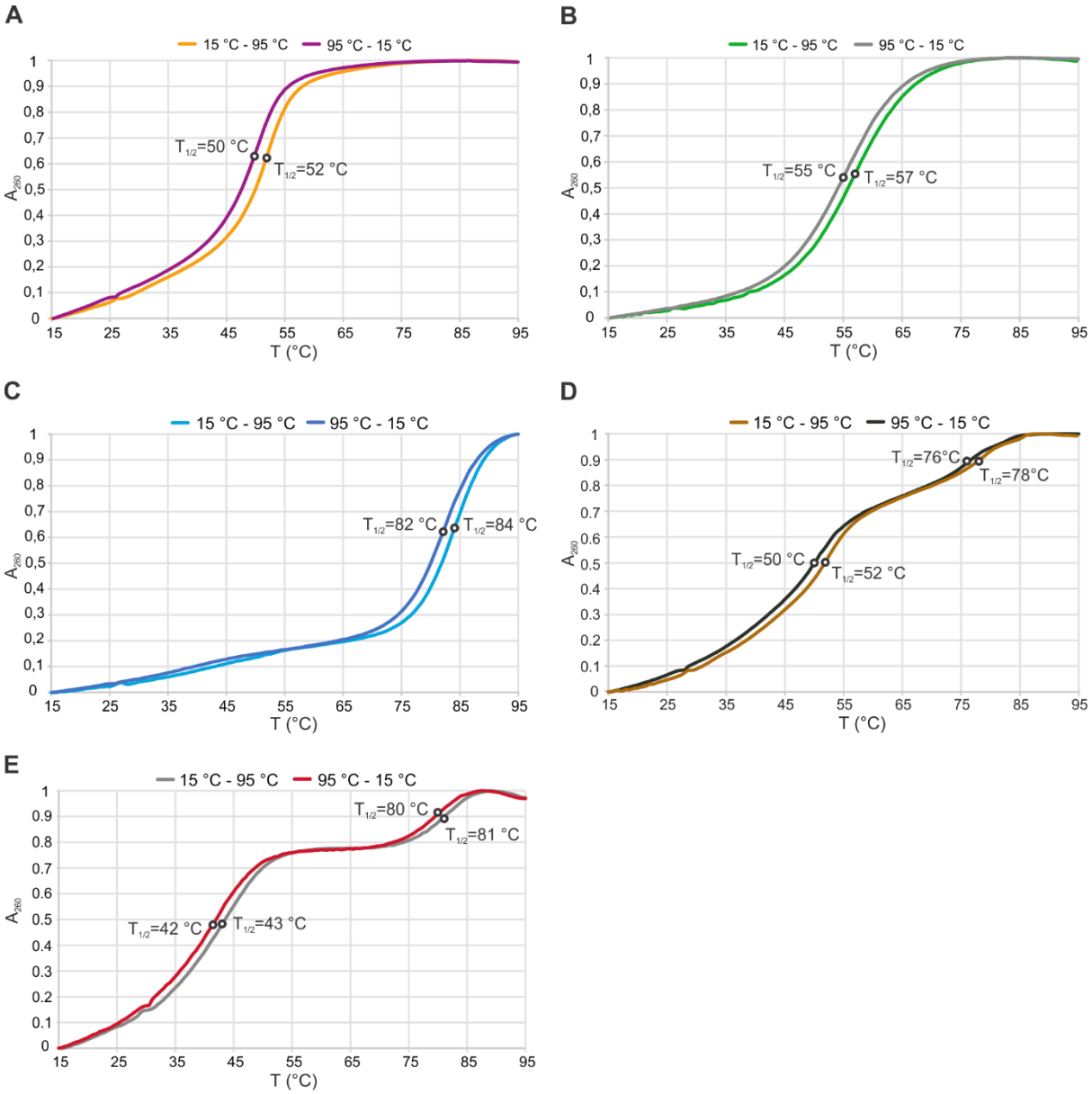

Figure S5. UV melting profiles of SL1, SL2, SL3, OxyS and SL4+SL3. **(A)**, **(B)**, **(C), (D), (E)** UV melting curves with melting temperatures (T_m) shown with black circles. In the case of SL4+SL3 and OxyS two melting temperatures were observed for each curve.

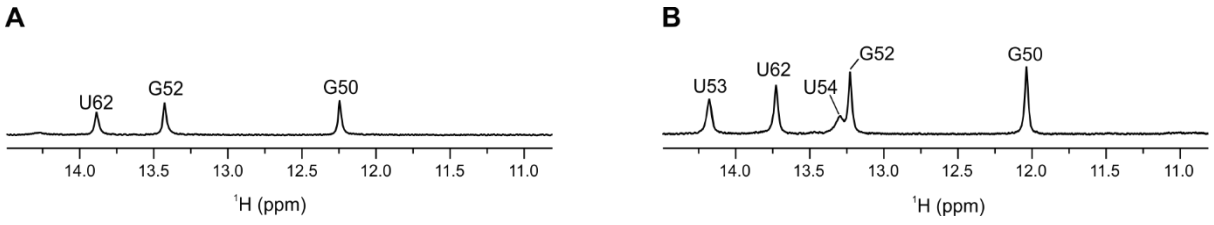

Figure S6. ^{1}H NMR spectrum of SL2. Three imino signals are present at **(A)** 25 °C and **(B)** five at 5 °C.

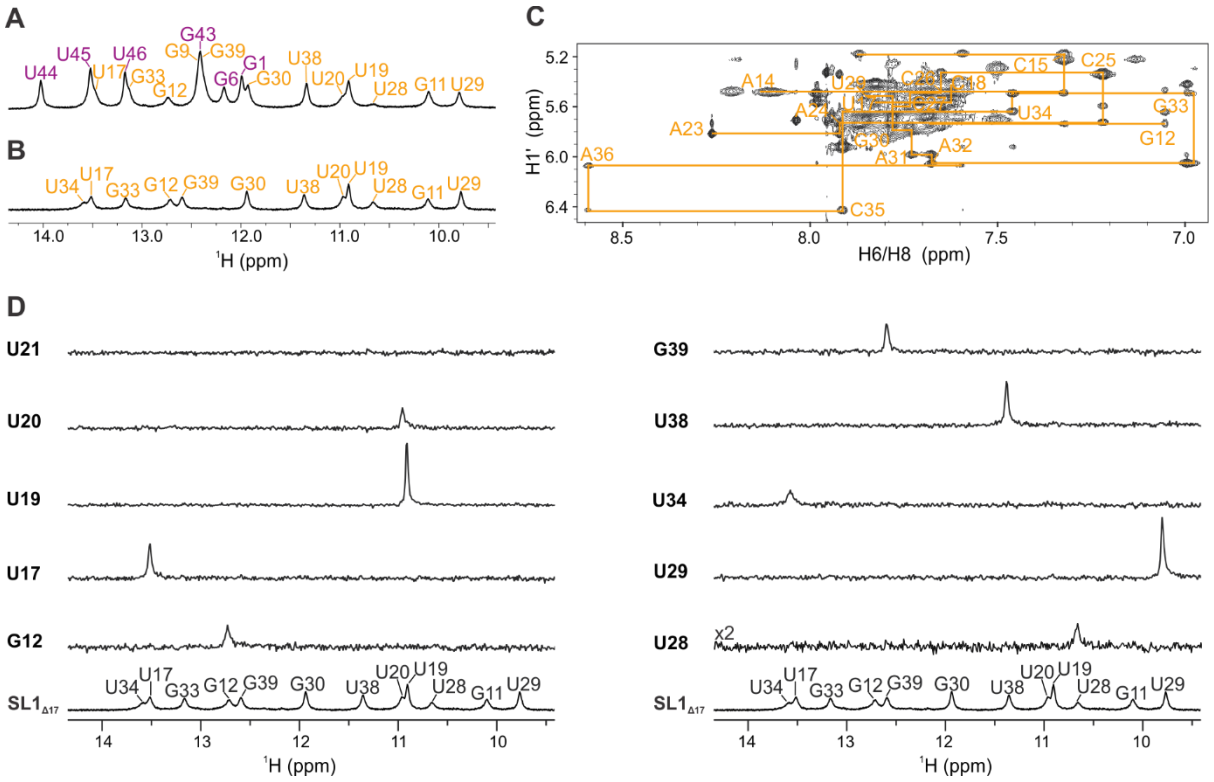

Figure S7. $SL1_{\Delta17}$ adopts the same secondary structure as SL1. **(A)** ^{1}H NMR spectrum of SL1 and **(B)** $SL1_{\Delta17}$ at 0 °C confirming the identical fold of both constructs. **(C)** Aromatic-anomeric region of a NOESY spectrum (τ_m = 250 ms) of $SL1_{\Delta17}$ at 15 °C, displaying the same pattern of sequential connectivities as SL1 (Fig. 3 D). **(D)** Imino region of a 1D ^{1}H NMR spectrum of $SL1_{\Delta17}$ and 1D ^{15}N-edited HSQC spectra of site-specific isotopically enriched $SL1_{\Delta17}$ oligonucleotides above. Spectra were acquired with 90 % H_2O and 10 % $^{2}H_2O$, 0.8 mM RNA concentration, 15 mM Na-phosphate buffer, 30 mM NaCl, and, pH 6, on a 600 MHz NMR spectrometer.

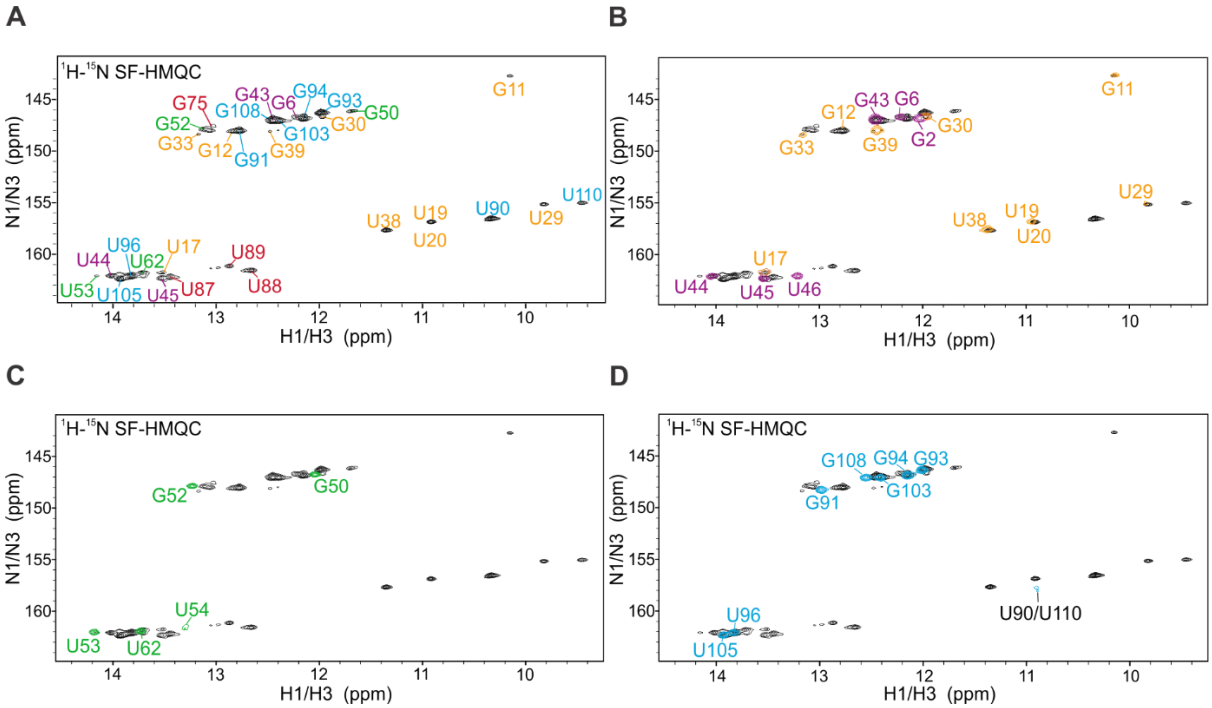

Figure S8. Overlaid ^{1}H-^{15}N SF-HMQC spectra of isolated stem-loops and ^{1}H-^{15}N B-TROSY of full-length OxyS. Evident similarities between the spectra strongly suggest structural integrity of stem-loops SL1, SL2 and SL3 is preserved within the full-length OxyS. **(A)** ^{1}H-^{15}N SF-HMQC spectra of full-length OxyS. The assignment is based on ^{1}H-^{15}N SF-HMQC spectra of isolated stem-loops shown in (B-D) and the analysis of NOESY spectra of full-length OxyS. **(B-D)** ^{1}H-^{15}N SF-HMQC spectrum of full-length OxyS overlaid with ^{1}H-^{15}N SF-HMQC spectra stem-loops SL1, SL2 and SL3 in orange-purple, green and blue, respectively. Spectra were acquired at 5 °C with 90 % H_2O and 10 % ^2H_2O, 15 mM Na-phosphate buffer, 30 mM NaCl, and, pH 6, on a 600 MHz NMR spectrometer. RNA concentrations ranged from 0.8 to 1.0 mM.

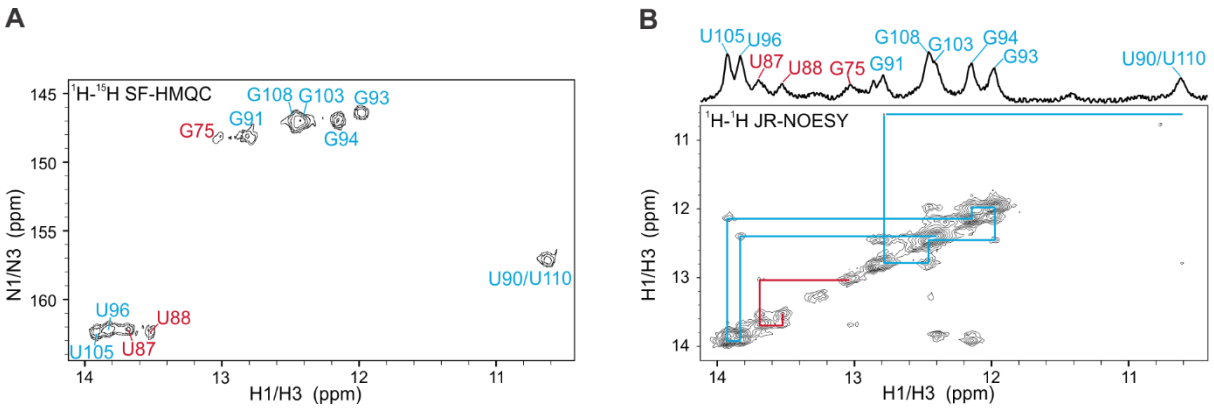

Figure S9. Structural characterization of SL4+SL3. Imino region of **(A)** ^{1}H-^{15}N SF-HMQC spectrum and **(B)** JR-NOESY spectrum (τ_m = 200 ms). Nucleotides corresponding to SL4 and SL3 are coloured in red and blue, respectively. Spectra were acquired at 5 °C with 90 % H_2O and 10 % $^{2}H_2O$, 0.4 mM RNA concentration, 15 mM Na-phosphate buffer, 30 mM NaCl, and, pH 6, on a 600 MHz NMR spectrometer.

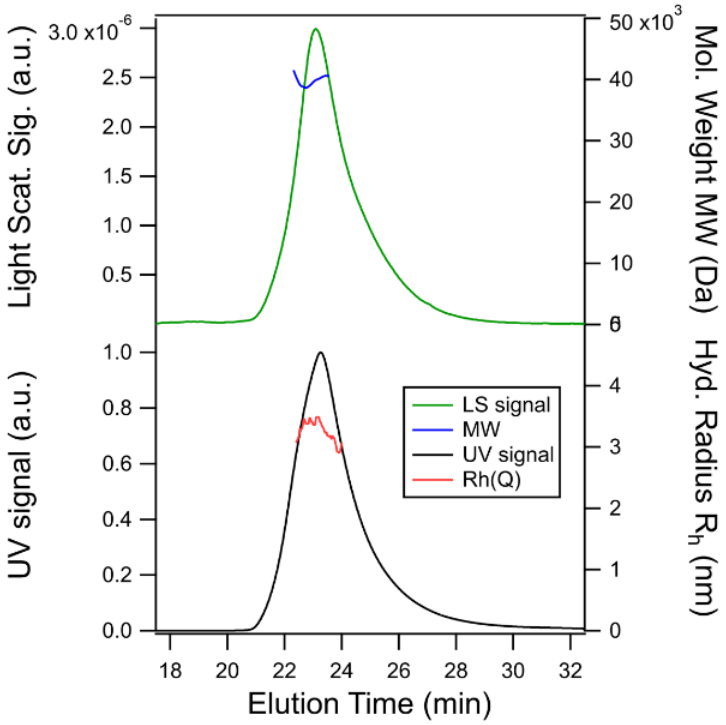

Figure S10. The SEC profile for the UV-VIS, LS signal the molecular weight (MW) and the hydrodynamic radius (R_h) in the peak regime of the RNA elution profile.

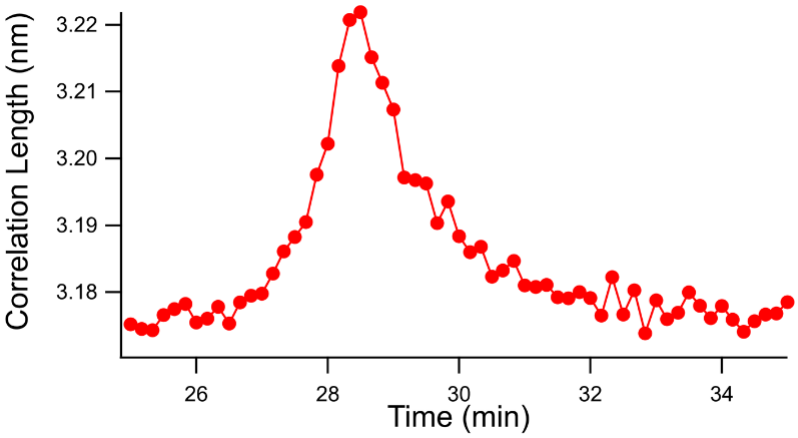

Figure S11. SAXS integral parameter correlation length (i.e. the first moment divided by the second moment of the scattering curve) of the non-subtracted SEC SAXS data versus elution time. The time off-set regarding the SEC data is given by the additional volume from the SEC system to the observation window of the SAXS capillary. The SEC SAXS pattern for OxyS has been averaged between 28 and 29.5 min.

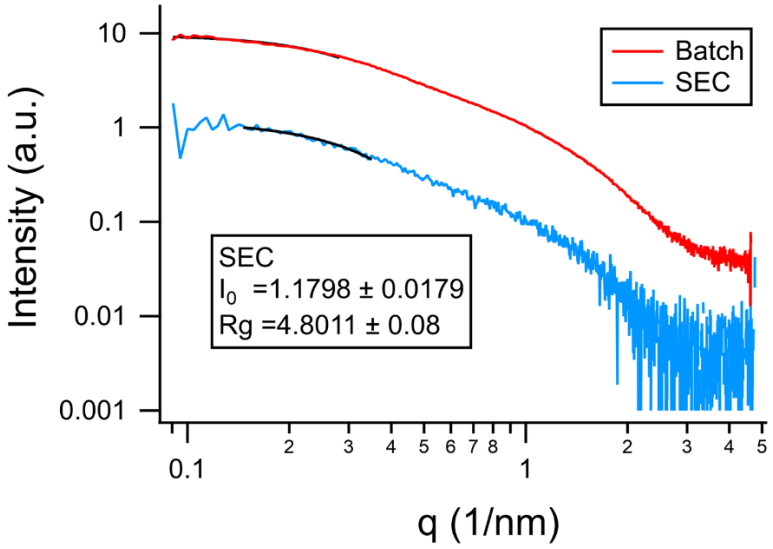

Figure S12. SAXS pattern of the measurements in the modes: batch and SEC (averaged over the SEC elution peak).

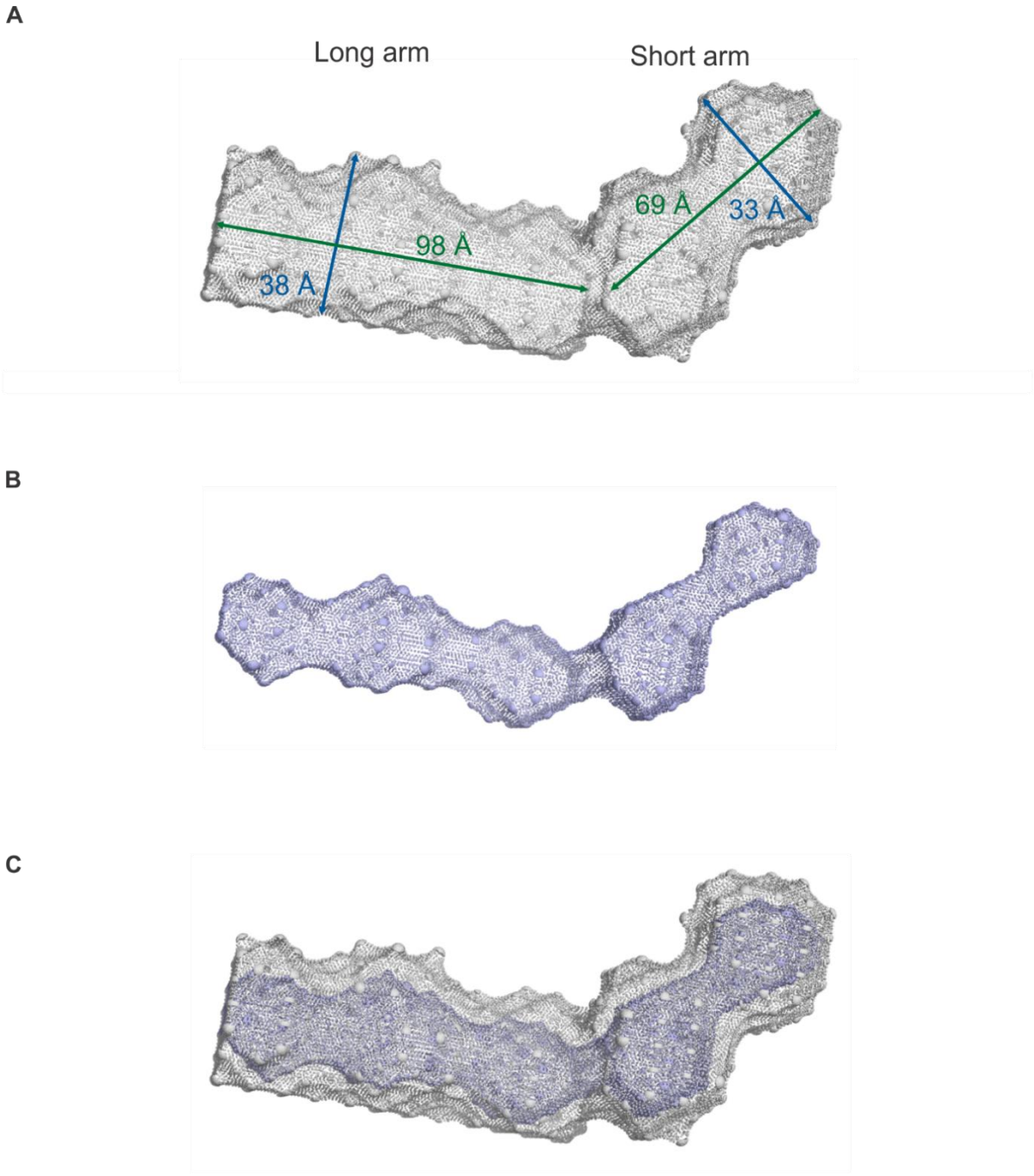

Figure S13. (A) The averaged envelope (*-avr.pdb) of the most representative cluster and its dimensions. **(B)** Envelope (*-flt.pdb) representing the compact - most probable - model of the representative cluster **(C)** The (*-avr.pdb) envelope and (*-flt.pdb) envelope overlaid.

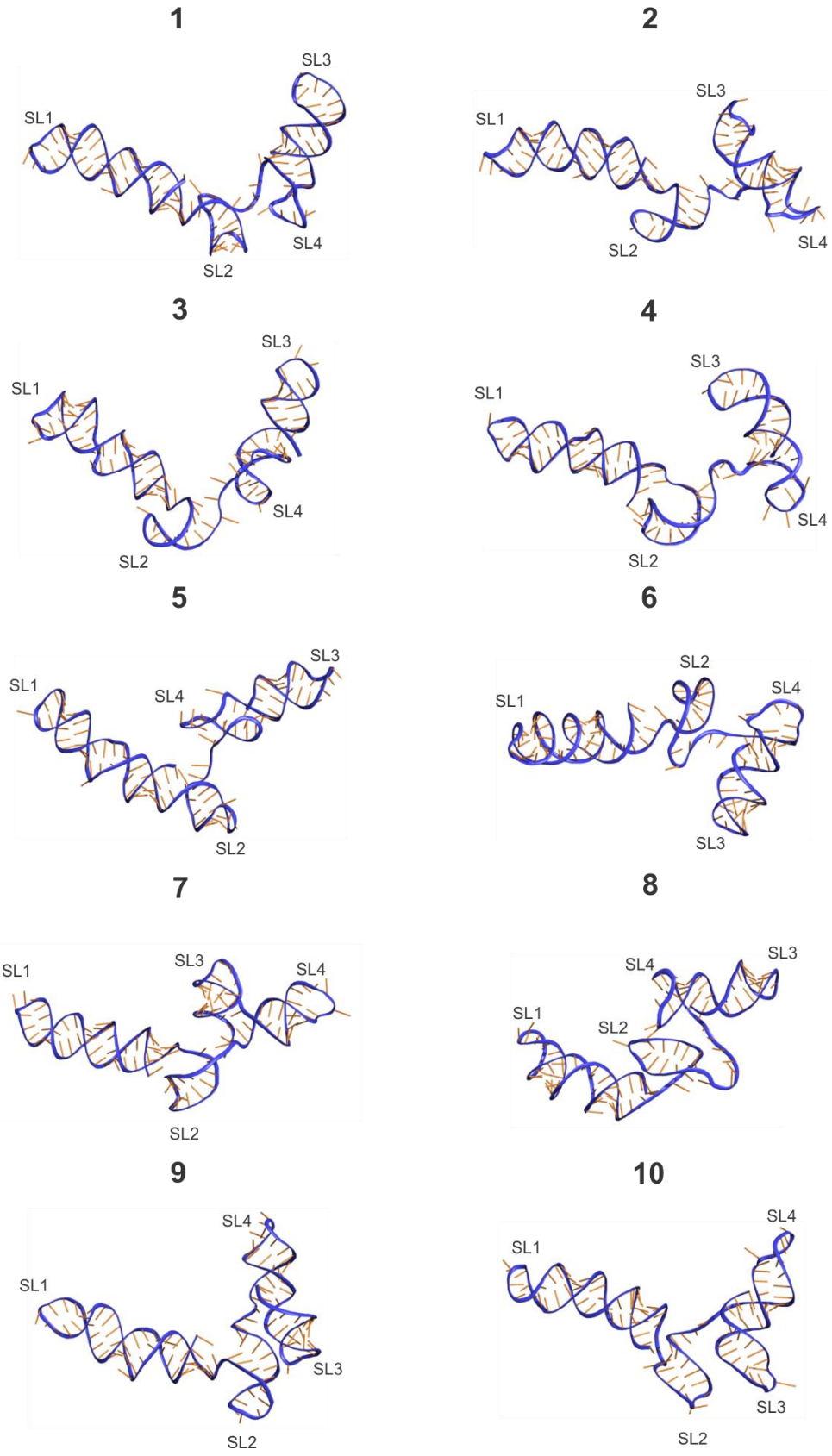

Figure S14. Structures of 10 best models from the FARFAR2 3D model prediction.

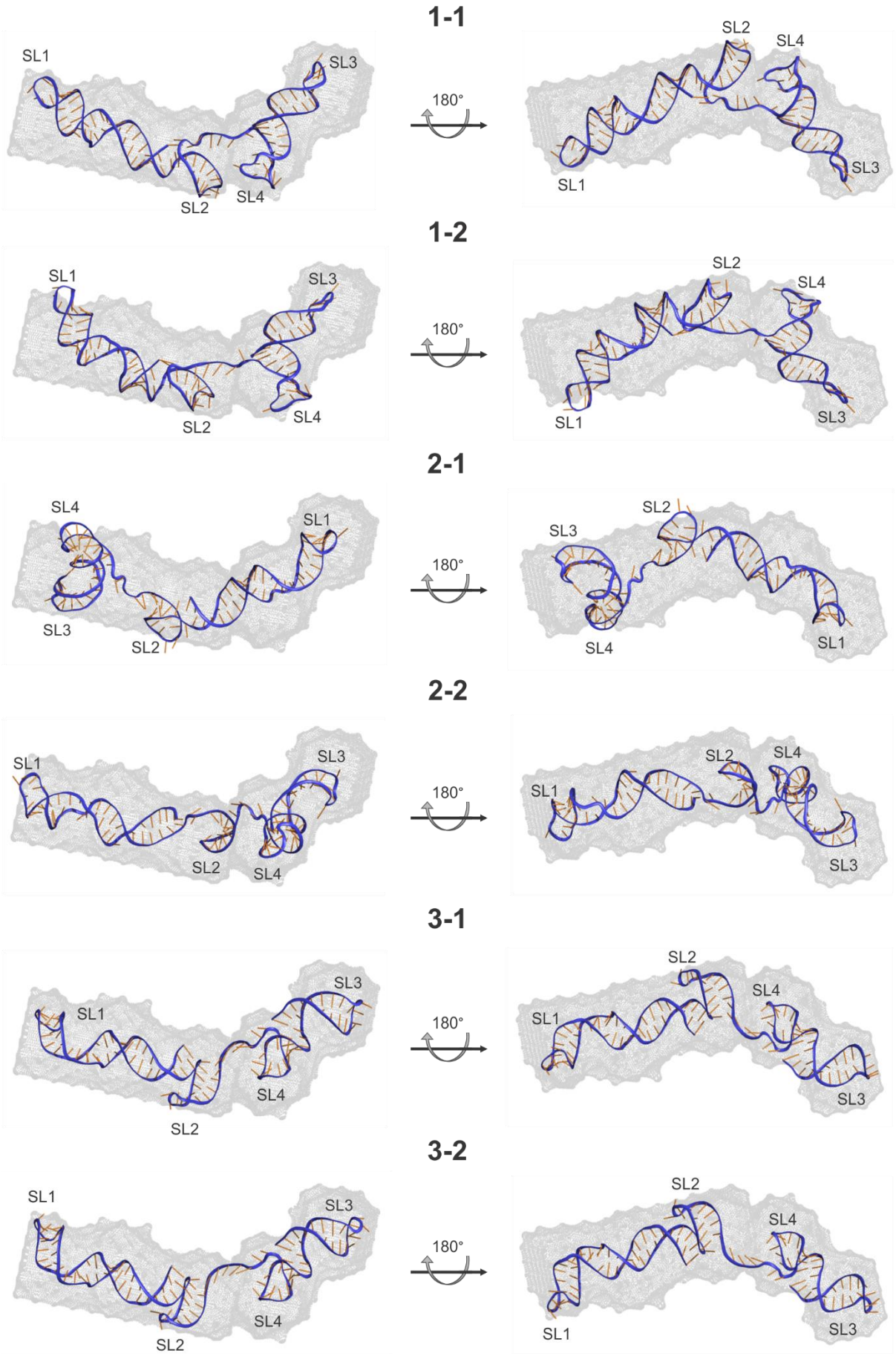
1-1
SL1
SL3
SL2
SL4
180°
SL2
SL4
SL3
SL1
1-2
SL1
SL3
SL2
SL4
180°
SL2
SL4
SL1
SL3
2-1
SL4
SL1
SL3
SL2
180°
SL2
SL3
SL4
SL1
2-2
SL1
SL3
SL2
SL4
180°
SL2
SL4
SL1
SL3
3-1
SL3
SL1
SL4
SL2
180°
SL2
SL4
SL1
SL3
3-2
SL1
SL3
SL4
SL2
180°
SL2
SL4
SL1
SL3

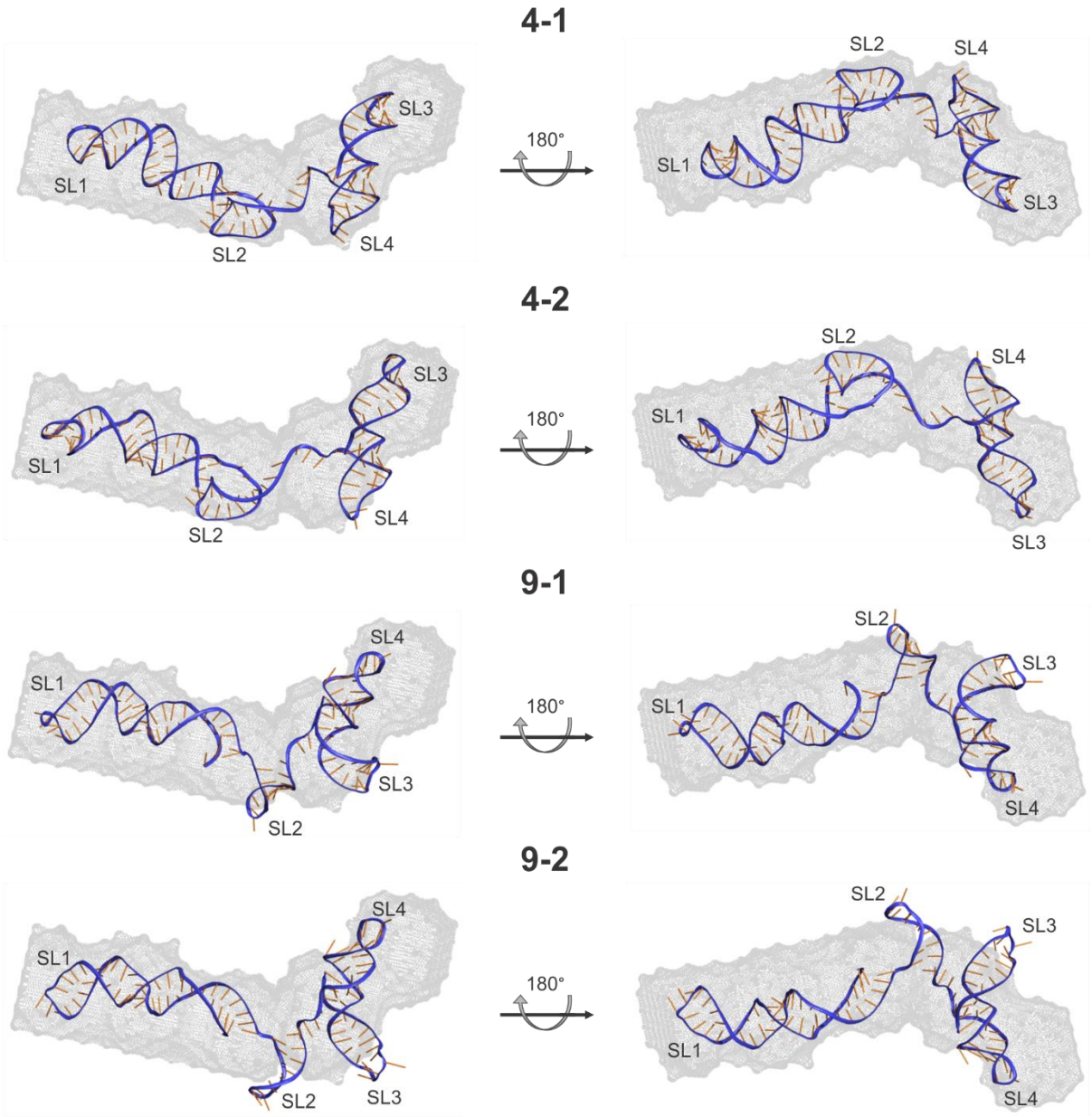

Figure S15. Ensemble of 10 3D models of OxyS (selected from the MD simulation trajectories) superimposed onto the molecular envelope (grey) using SUPCOMB.

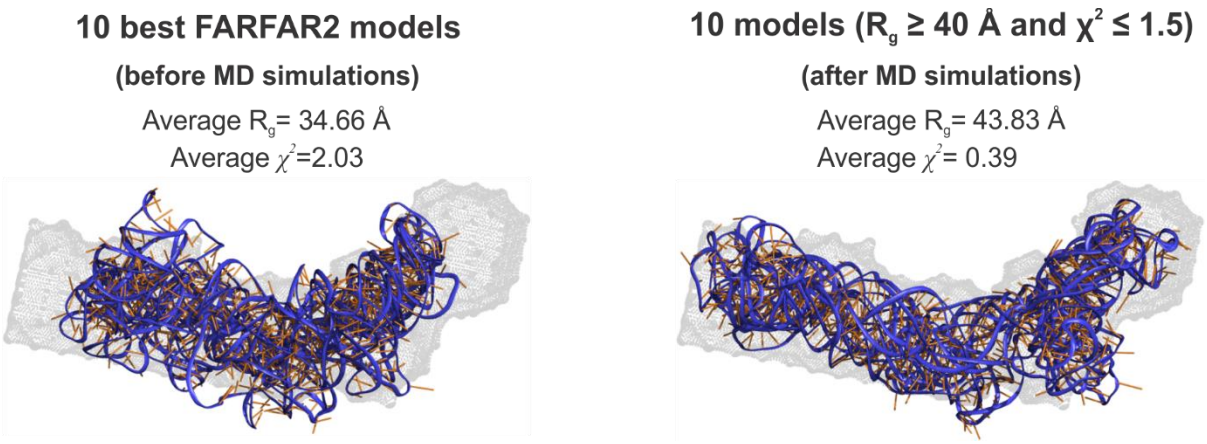

Figure S16. 10 best FARFAR2 models (before MD) and the 10 models selected from simulation trajectories (after MD) superimposed onto the averaged envelope of the most representative cluster (shown in grey). The improved fit of the models in the final ensemble is reflected in their agreement with the shape defined by the averaged envelope and in the average R_g and χ^2 values.

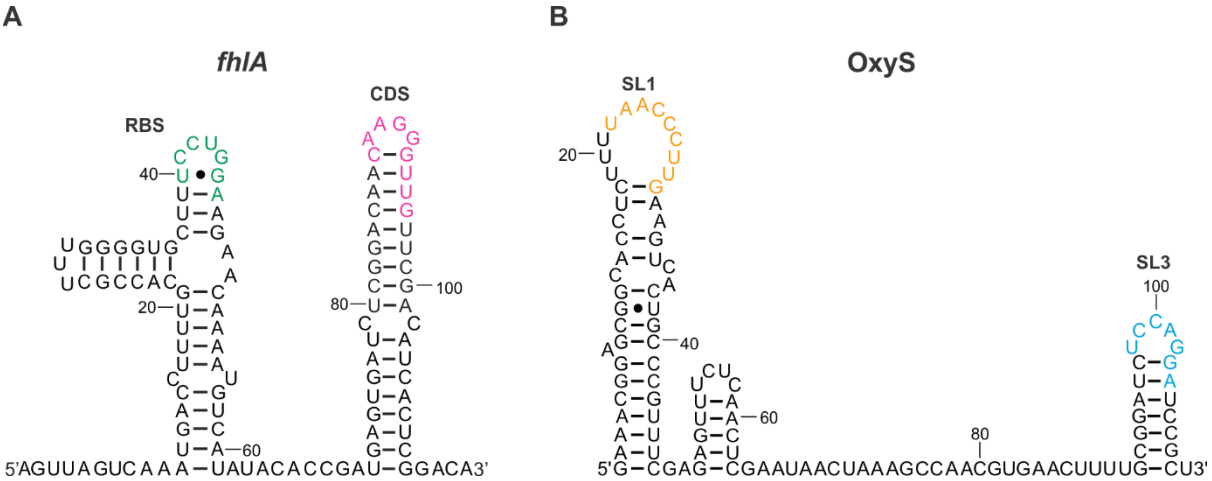

Figure S17. Sites of interaction between OxyS sRNA and 5' UTR of *fhlA* mRNA are denoted on the predicted structures. **(A)** Nucleotides from *fhlA* expected to interact with OxyS are coloured in green and magenta. **(B)** Nucleotides from OxyS expected to interact with OxyS are coloured in orange and blue.

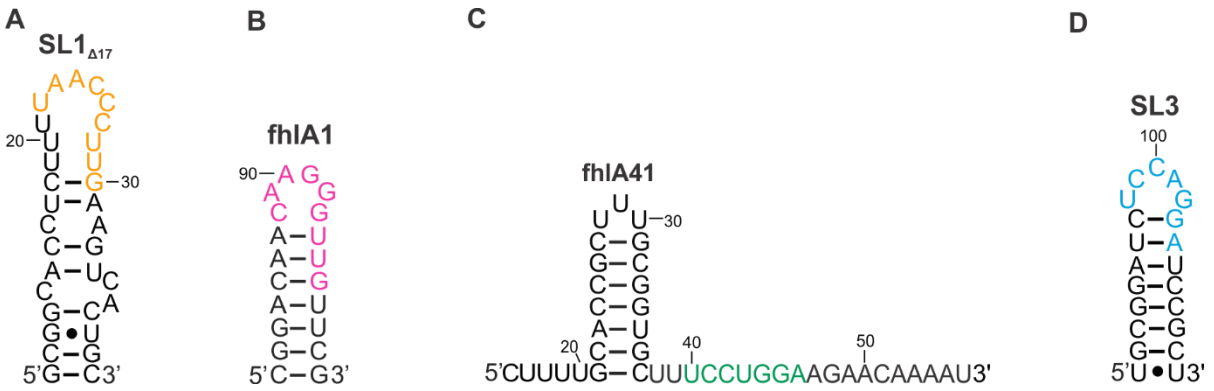

Figure S18. Constructs used for the NMR study of OxyS-*fhlA* interaction. Experimentally determined secondary structures of **(A)** $SL1_{\Delta17}$, **(B)** fhlA1, **(C)** fhlA41 and **(D)** SL3. Nucleotides expected to be involved in the formation of the OxyS-*fhlA* complex are coloured in orange, magenta, green and blue.

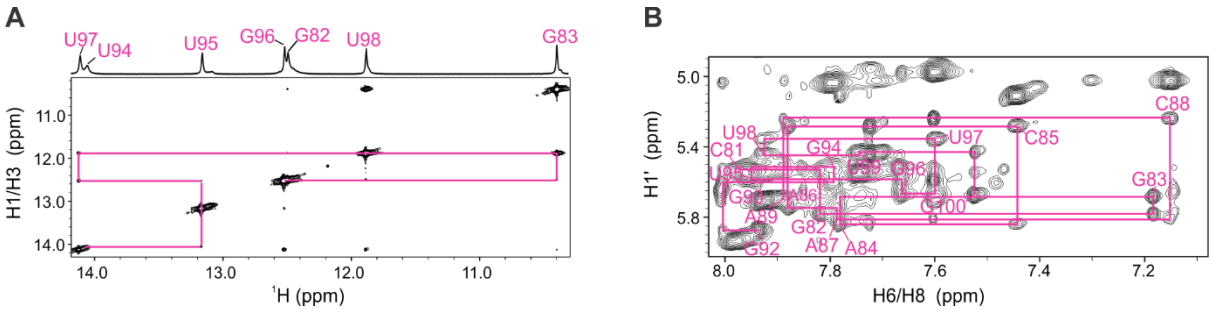

Figure S19. NMR characterization of fhlA1. **(A)** Imino region of a NOESY spectrum (τ_m = 200 ms) acquired at 25 °C. Imino-imino walk is denoted with lines coloured in magenta. **(B)** Aromatic-anomeric region of a NOESY spectrum (τ_m = 200 ms) acquired at 25 °C, denoting sequential connectivities with lines coloured in magenta. Spectra were acquired with 90 % H_2O and 10 % ^2H_2O, 1.3 mM RNA concentration, 15 mM Na-phosphate buffer, 30 mM NaCl, 5 mM $MgCl_2$ and, pH 6, on a 600 MHz NMR spectrometer.

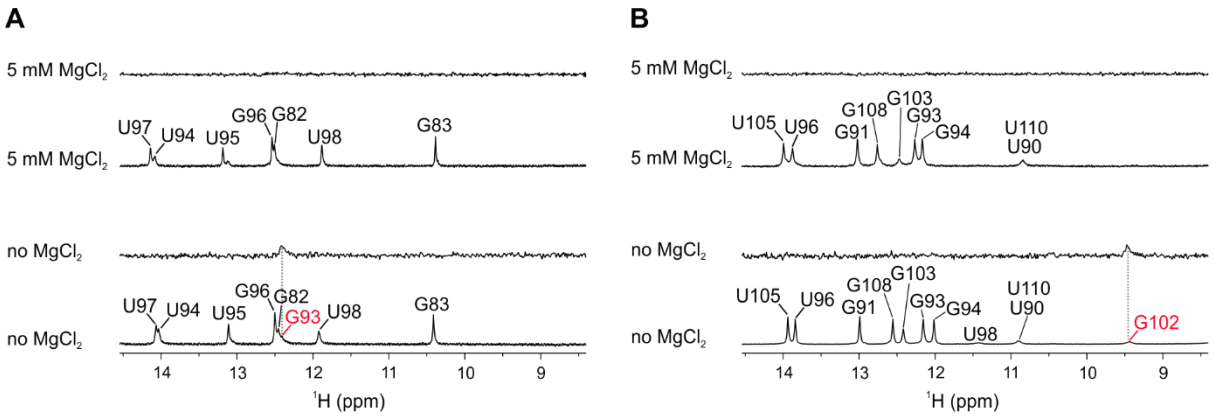

Figure S20. The addition of $MgCl_2$ influences the structure of constructs used in the interaction. **(A)** In the proton NMR spectra of fhlA1, the imino signal of G93 from the closing G·C base pair is no longer present after the addition of 5 mM $MgCl_2$. **(B)** In the proton NMR spectra of SL3, the imino signal of G102 from the closing G·U base pair disappears after the addition of 5 mM $MgCl_2$. Spectra were acquired at 5 °C, with 90 % H_2O and 10 % ^2H_2O, 0.5 mM RNA concentration, 15 mM Na-phosphate buffer, 30 mM NaCl, 5 mM $MgCl_2$ and, pH 6, on a 600 MHz NMR spectrometer.

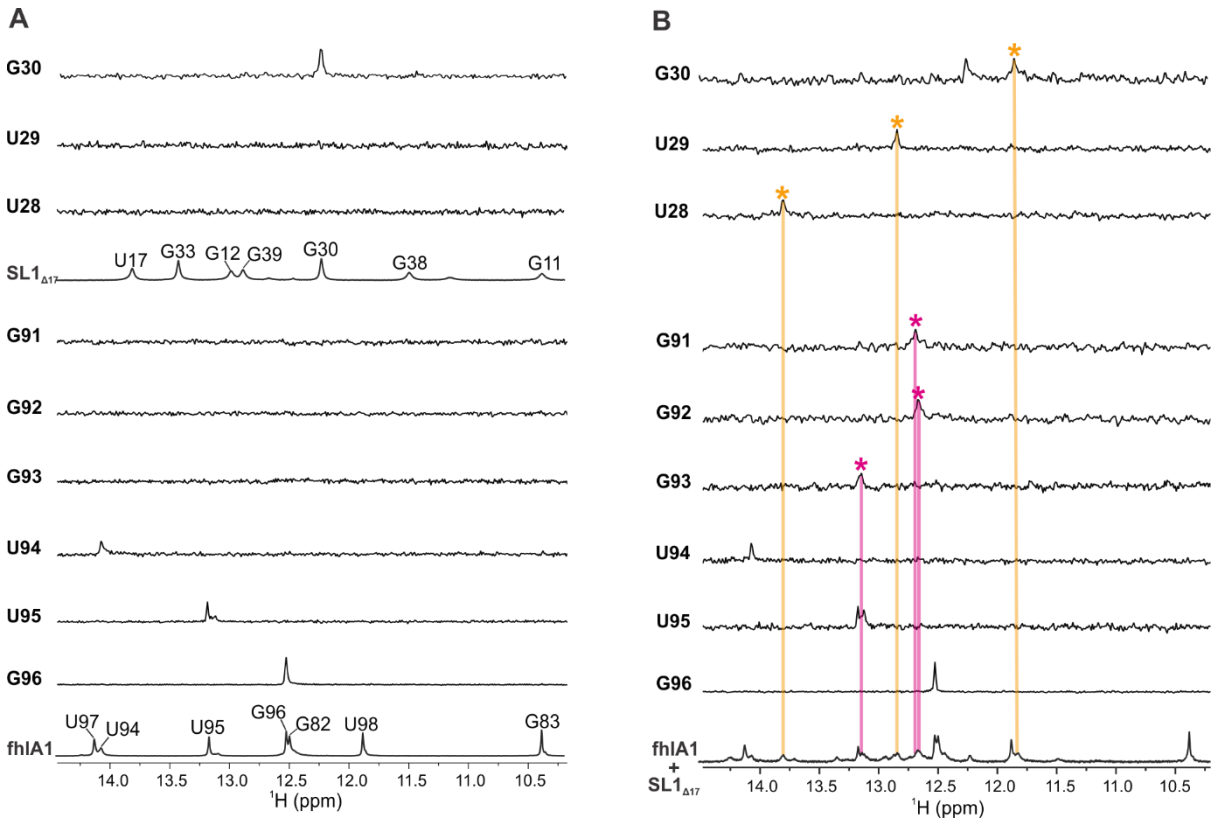

Figure S21. NMR characterization of interaction complex at *fhlA* 5' UTR. **(A)** Imino region of a 1D ^{1}H NMR spectrum of fhlA1 and SL1$_{\Delta17}$ and 1D ^{15}N-edited HSQC spectra of site-specific isotopically enriched fhlA1 and SL1$_{\Delta17}$ oligonucleotides above. **(B)** Imino region of a 1D ^{1}H NMR spectrum of fhlA1 and SL1$_{\Delta17}$ mixed in equimolar ratio (fhlA1+SL1 $_{\Delta17}$) and above it 1D ^{15}N-edited HSQC spectra of samples in which one of the interacting sequences is site-specific isotopically enriched. New imino signals resulting from base pair formation in the OxyS-fhlA complex are denoted with an asterisk and a line colored in orange for SL1 $_{\Delta17}$ and magenta for fhlA1. Spectra were acquired at 25 °C with 90 % H_2O and 10 % $^{2}H_2O$, 15 mM Na-phosphate buffer, 30 mM NaCl, 5 mM $MgCl_2$ and, pH 6, on a 600 MHz NMR spectrometer. RNA concentrations were set to 0.2 mM per strand.

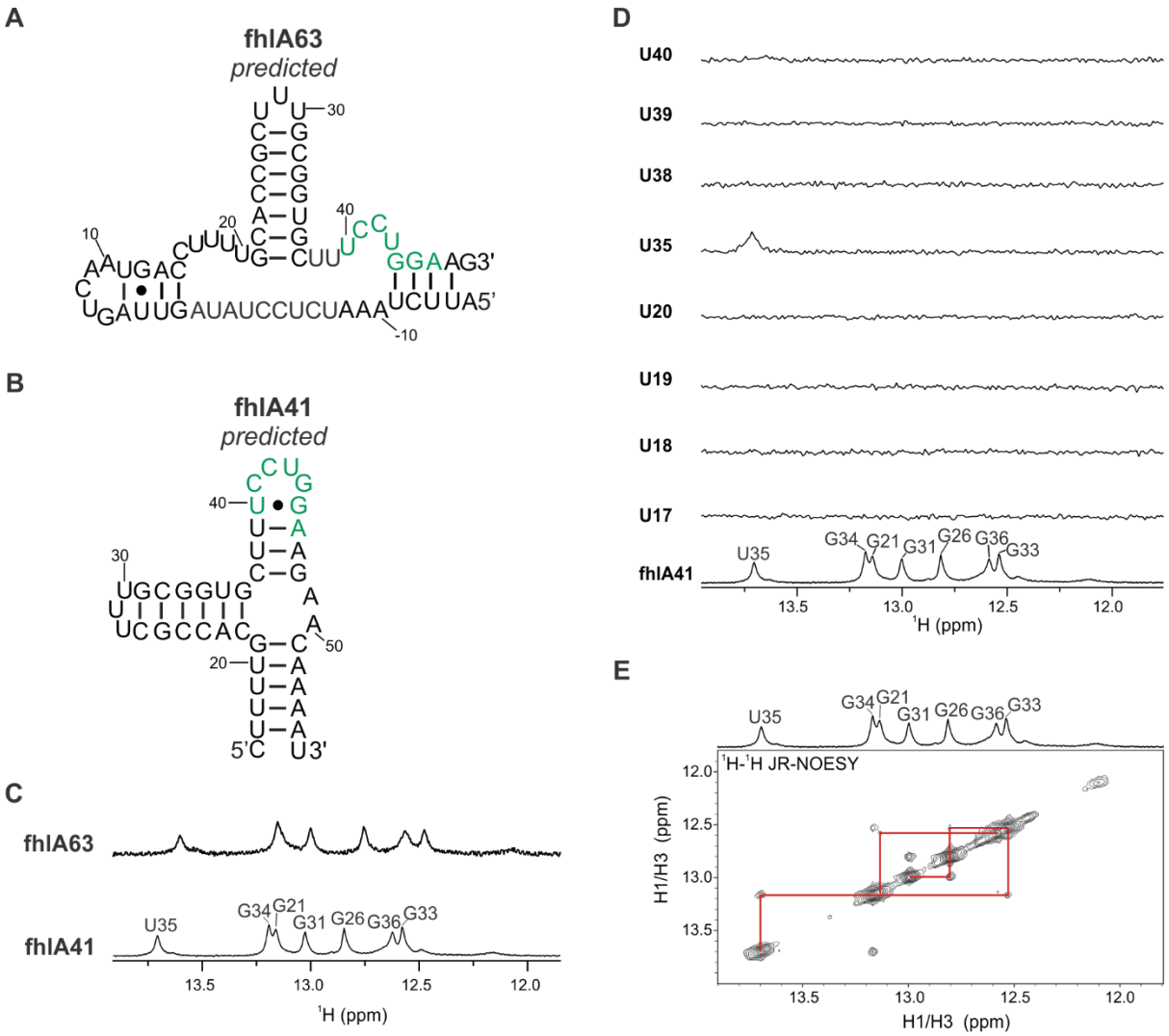

Figure S22. NMR characterization of model sequence fhlA41. **(A)** Predicted structure of fhlA63. **(B)** Predicted structure of fhlA41. **(C)** ^{1}H NMR spectra of fhlA63 and fhlA41 at 25°C confirm identical fold of both constructs. **(D)** Imino region of a 1D ^{1}H NMR spectrum of fhlA41 and 1D ^{15}N-edited HSQC spectra of site-specific isotopically enriched fhlA41 oligonucleotides. **(E)** Imino region of a JR-NOESY spectrum (τ_m = 200 ms) of fhlA41. Spectra were acquired at 25 °C with 90 % H_2O and 10 % $^{2}H_2O$, 15 mM Na-phosphate buffer, 30 mM NaCl, 5 mM $MgCl_2$ and, pH 6, on a 600 MHz NMR spectrometer. RNA concentrations varied from 0.25 mM to 0.45 mM.

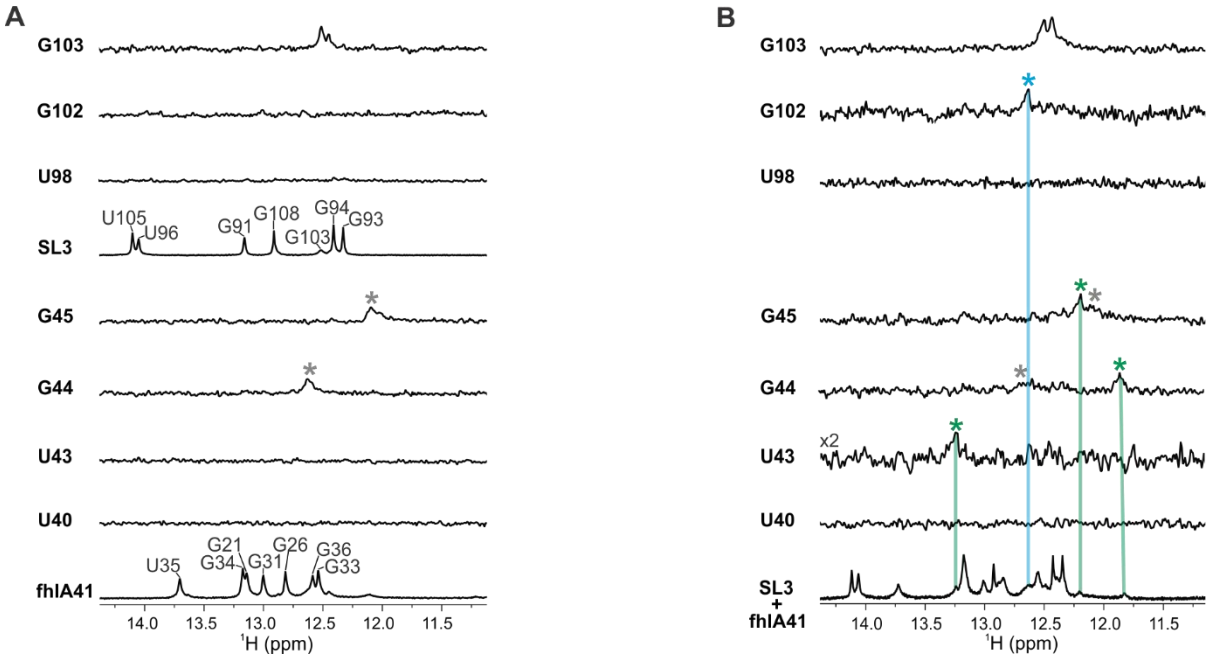

Figure S23. NMR characterization of interaction complex at *fhlA* 3' UTR. **(A)** Imino region of a 1D ^{1}H NMR spectrum of fhlA41 and SL3 with 1D ^{15}N-edited HSQC spectra of site-specific isotopically enriched fhlA41 and SL3 oligonucleotides above. Grey asterisks indicate the signals originating from two weak G·C base pairs in the minor dimeric species, which is present in a very small amount. **(B)** Imino region of a 1D ^{1}H NMR spectrum of SL3+fhlA41 and above 1D ^{15}N-edited HSQC spectra of SL3+fhlA41 samples in which one of the interacting sequences is site-specifically isotopically enriched above. New imino signals resulting from base pair formation in the OxyS-*fhlA* complex are denoted with an asterisk and a line coloured in green for fhlA41 and blue for SL3. Grey asterisks indicate the signals originating from two weak G·C base pairs in the minor dimeric species which are still present in the mixture since the minor species is not involved in the interaction. This is expected, as the interacting nucleotides are single-stranded in the main monomeric species and therefore free to interact, while they are already base paired in the minor dimeric species. Spectra were acquired at 25 °C with 90 % H_2O and 10 % $^{2}H_2O$, 15 mM Na-phosphate buffer, 30 mM NaCl, 5 mM $MgCl_2$ and, pH 6, on a 600 MHz NMR spectrometer. RNA concentrations were set to 0.2 mM per strand with an exception for sample SL3+fhlA41 with labelled U43 where concentration was 0.075 mM per strand.

Table S1. Nucleotide sequences of samples used in NMR study. Nucleotides added to enable *in vitro* transcription and enzymatic linearization of OxyS are in bold. Nucleotides which were added at the 5' and 3' end of individual stem loops to protect the terminal base pair from exchange with solvent are underlined.

Sample name	**Sequence**
OxyS	5'**G**GAAACGGAGCGGCACCUCUUUUAACCCUUGAAGUCACUGCC CGUUUCGAGAGUUUCUCAACUCGAAUAACUAAAGCCAACGUGAA CUUUUGCGGAUCUCCAGGAUCCGCU**A**3'
SL1	5'UGAAACGGAGCGGCACCUCUUUUAACCCUUGAAGUCACUGCCC GUUUCU3'
$SL1_{\Delta 17}$	5'GCGGCACCUCUUUUAACCCUUGAAGUCACUGC3'
SL2	5'AGAGUUUCUCAACUCG3'
SL3	5'UGCGGAUCUCCAGGAUCCGCU3'
$SL3_{ext}$	5'UUGCGGAUCUCCAGGAUCCGCUA3'
fhlA1	5'CGGACAACAAGGGUUGUUCG3'
fhlA41	5'CUUUUGCACCGCUUUGCGGUGCUUUCCUGGAAGAACAAAAU3'
fhlA63	5'AUUCUAAAUCUCCUAUAGUUAGUCAAUGACCUUUUGCACCGCU UUGCGGUGCUUUCCUGGAAG3'
SL4	5'UAAAGCCAACGUGAACUUUU3'
SL4+SL3	5'UAAAGCCAACGUGAACUUUUGCGGAUCUCCAGGAUCCGCUA3'

Table S2. Parameters of SAXS data acquisition.

Detector	Pilatus3 1M (Dectris)
Sample to Detector Distance	1501 mm
Beamsize:	0.4 x 3 mm^2 (µdrop-Batch) 0.25 x 2 mm^2 (SEC/Capillary-Batch)
Exposure Times	18 x 10s (µdrop-Batch) 18 x 10s (Capillary-Batch) 10s (SEC)
SEC Column	Supradex 75 Increase 10/300 GL
SEC-SAXS set-up	- HPLC Agilent 1260II Infinity (Agilent), - multisampler Bio-Inert 1260 Infinity II (Agilent), - UV-vis 1260 Infinity II (Agilent), - QELS-DAWN autocorrelator (Wyatt), - Multi Angle laser scattering DAWN18 (Wyatt), - Optilab Detector (Wyatt), - Software for data evaluation Astra8 (Wyatt)

Table S3. Summary of the derived SAXS data.

Parameter	OxyS
Guinier Analysis	
R_g (nm)	4.76 ± 0.38
I(0) (a.u./cm^{-1})	9.67 ± 0.35
q-range (nm^{-1})	0.22–0.39
Quality (%)	96
GNOM	
Max. dimension D_{max} (nm)	15.5
Guinier radius R_g (nm)	4.63 ± 0.03
I(0) (a.u./cm^{-1})	9.38 ± 0.07
q-range (nm^{-1})	0.13–1.87
Molecular Weight Vc (kDa)	38.768
Q_{max} (nm^{-1})	3.0
DAMMIF (def. parameter, 10 runs)	
q range for fitting (nm^{-1})	0.13–1.87
Symmetry, anisotropy assumption	P1, unknown
χ^2 range	0.515-0.54
Resolution from SASRES (nm)	5
NSD (standard dev.), no. of clusters	0.933+/-0.187, 4
MW estimate for proteins (kDa)	38930+/-880
Phase radius of gyration (nm)	4.63+/-0.056
Maximum phase diameter (nm)	15.500
SASBDB code	SASDQP8

Table S4. The OxyS nucleotide sequence and dot-bracket secondary structure annotation were used as input for the Rosetta FARFAR2.

```
GGAAACGGAGCGGCACCUCUUUUAACCCUUGAAGUCACUGCCCGUUUCGAGAGUUUCUCAACUCGAAUAACUAAAGCCAACGUGAACUUUUGCGGAUCUCCAGGAUCCGCUA
.(((((((.((((.((.((...........)).)).))))))))))..(((((....)))))........((((..........)))).(((((((.....)))))))..
```

Table S5. R_g (Å) and χ^2 values of 10 best models from the FARFAR2 3D model prediction. The models are listed based on their fit (χ^2) to the experimental SAXS data.

FARFAR2 model name	**R_g (Å)**	**χ^2**
1	36.22	0.99
2	36.78	1.50
3	35.48	1.76
4	36.20	1.92
5	34.35	1.96
6	33.85	2.15
7	34.43	2.32
8	33.03	2.50
9	33.18	2.57
10	33.11	2.61

Table S6. Rg (Å) and χ^2 values of 10 OxyS 3D models selected from the simulation trajectories (trajectories 1, 2, 3, 4 and 9) which satisfied our selection criteria ($R_g \geq 40$ Å and $\chi^2 \leq 1.5$). First number in the model name denotes which FARFAR2 model/trajectory (Table S5) was used as the starting structure, and the second number is either 1 for model which had lowest χ^2 value in the trajectory or 2 for model with R_g closest to the experimentally determined value. The five models (1-2, 2-1, 3-1, 4-2, 9-2) in the final ensemble obtained by NNLSJOE are in bold.

Model name	**Rg (Å)**	**χ^2**
1-1	42.75	0.14
1-2	**43.84**	**0.58**
2-1	**43.54**	**0.15**
2-2	46.85	0.50
3-1	**45.20**	**0.12**
3-2	46.90	0.68
4-1	40.67	0.26
4-2	**45.23**	**0.53**
9-1	41.64	0.40
9-2	**41.63**	**0.56**

Table S7. Results of the ensemble optimization with the ATSAS program NNLSJOE. NNLSJOE is a program for the selection of an ensemble of models, whose combined theoretical scattering intensity best describe the experimental SAXS data. Shown are the relative fractions of the models, R_g and D_{max} values, molecular weight (MW) and the fraction weighted hydrodynamic radius (R_h). R_h was calculated with the software package US-SOMO (Brookes and Rocco 2023).

Model name	**Fraction**	**R_g (Å)**	**D_{max} (Å)**	**MW (Da)**	**R_h (nm)**
1-2	0.06	42.7	132.5	3.57E+04	3.63
2-1	0.28	42.9	144.4	3.57E+04	3.63
3-1	0.03	44.5	153.8	3.57E+04	3.62
4-2	0.12	44.5	138.7	3.57E+04	3.62
9-2	0.50	40.8	138.7	3.57E+04	3.56

Average R_h=3.59 nm

χ^2 = 0.22 (for the final ensemble of 5 models)

REFERENCES

Brookes EH, Rocco M. 2023. Beyond the US-SOMO-AF database: a new website for hydrodynamic, structural, and circular dichroism calculations on user-supplied structures. *Eur Biophys J*.

Zuker M. 2003. Mfold web server for nucleic acid folding and hybridization prediction. *Nucleic Acids Res* **31**: 3406–3415.